U and Th zonation in Fish Canyon Tuff zircons:

Implications for a zircon (U-Th)/He standard

Katherine J. Dobson[*1,2], Finlay M. Stuart[2], Tim J. Dempster[1] & EIMF[3]

[1]Geographical & Earth Sciences, University of Glasgow, Gregory Building, Glasgow G12 8QQ, UK

[2]S.U.E.R.C., Rankine Avenue, Scottish Enterprise Technology Park, East Kilbride G75 0QF. UK

[3]NERC Ion Microprobe Facility, Grant Institute, University of Edinburgh. Edinburgh. EH9 3JW. UK

* Corresponding author: (Kate.Dobson@ges.gla.ac.uk)

Revised manuscript submitted 17th July 2008

ABSTRACT

The inability to accurately determine the distribution of U and Th in zircon crystals analysed using (U-Th)/He is a major source of error, and limits the confidence in subsequent data interpretation. The Fish Canyon Tuff (FCT) zircon standard shows (U-Th)/He age reproducibility in excess of ± 10 %. We have tested the extent to which this is due to U and Th zonation using a combination of cathodoluminescence and ion probe analysis of a population of FCT zircons. Primarily we find that FCT zircons exhibit extreme U and Th zonation, and the population has large inter-crystalline variability. Furthermore, the net cathodoluminescence intensity from the FCT zircons is negatively correlated with U and Th concentration, allowing cathodoluminescence emission to be used as a proxy for U and Th zonation. This correlation was exploited to constrain the U and Th zonation within the crystal population, and to show that the poor age reproducibility of the FCT zircons is consistent with the observed zonation.

1. INTRODUCTION

The development of the zircon (U-Th)/He thermochronometer allows constraint of cooling histories over a time-temperature range that is difficult to resolve using existing techniques. With a closure temperature of ~180-200ºC (Reiners et al., 2004), zircon (U-Th)/He dating has potential applications in constraining shallow- and mid-crustal cooling events from a wide range of geological settings.

Helium loss from zircon is governed by two processes: thermally-activated volume diffusion, and the ejection of ^{4}He, caused by the high kinetic energy of α-particles produced by ^{238}U-, ^{235}U- and ^{232}Th-decay. These α-particles move 10-20μm through the crystal lattice, and a proportion of those generated in the outermost regions of the crystal are lost from subsequent measurement (Farley et al., 1996).

For rapidly cooled samples, diffusive loss can be considered to be negligible, and all He loss is though α-ejection. When a crystal has a homogeneous distribution of U and Th, the proportion of He lost by α-ejection can be calculated using the empirical relationship between fractional retention and the surface area-to-volume ratio of the crystal (Farley et al., 1996; Hourigan et al., 2005). However, strong zonation of U and Th is common in zircon and can change the fractional loss of He due to α-ejection (Hourigan et al., 2005; Tagami et al., 2003). Modelling of simple zonation profiles has shown that errors of up to 30% can be introduced into the ejection corrected He age if zonation is not considered (Hourigan et al., 2005).

(U-Th)/He ages of apatite and zircon are usually reported relative to a mineral age standard. The accuracy of unknown ages is determined from the 2σ uncertainty on the average age of numerous determinations on a standard (Farley, 2002). Analysis of mineral age standards also provides a relatively simple way of assessing the integrity

of a laboratory's procedures. Age standards are typically derived from rapidly-cooled rocks in order to minimise complexities introduced by diffusive loss of noble gas daughter isotopes (i.e. ^{4}He and ^{40}Ar). Zircon from the Fish Canyon Tuff (FCT) is the only widely-used standard for zircon (U-Th)/He thermochronometry (Reiners, 2005). FCT zircons are typically less than 250 μm long and less than 150μm wide and so whole crystals are required for (U-Th)/He analysis. Substantial (typically up to 30%) α-ejection corrections are therefore required. The average ejection-corrected zircon (U-Th)/He age from all laboratories routinely performing analyses (28.3 ± 3.1 Ma, Fig. 1) is within the uncertainty of ages obtained by other techniques, but the He age reproducibility is ± 10.9 % (2σ, n = 127), significantly beyond typical analytical uncertainties.

Significant U and Th zonation has been observed in FCT zircons (e.g. Schmitz and Bowring, 2001) and it has been suggested that this may cause the poor He age reproducibility (Reiners et al., 2002). Understanding the effects of U and Th zonation on α-ejection in FCT zircon is crucial for accurate interpretation of all zircon (U-Th)/He data. Here we demonstrate that U and Th zonation in FCT zircon correlates strongly with CL emission intensity, thereby allowing the effect of zonation on α-ejection, and on the FCT (U-Th)/He age population to be quantified.

2. CATHODOLUMINESCENCE (CL) ZONATION IN FCT ZIRCONS

2.1. CL zonation patterns in FCT zircon

Zircons are commonly divided into "blue" and "yellow" groups based on broad-band CL emission peaks centred at ~360 nm and ~560 nm respectively (Remond et al., 1992; Kempe et al., 2000; Nasdala et al., 2003). Narrow-band CL emission, often

associated with rare earth element (REE) 3^+ centres, is superimposed upon this underlying broad-band signal. Specific luminescence centres can be identified from the wavelength of narrow-band emission peaks (Edwards et al., 2007; Ewing et al., 2003; Nasdala et al., 2003), but the origin of the broad-band CL and the mechanisms controlling intensity remain poorly understood (Kempe et al., 2000; Ewing et al., 2003; Nasdala et al., 2003). However, correlations between areas of high density radiation damage and areas of low CL intensity are widely reported (Ewing et al., 2003; Hanchar and Miller, 1993; Nasdala et al., 2003). α-decay of U and Th is the dominant source of lattice damage in zircon (Ewing et al., 2003), and the reported correlation implies that while U and Th are not directly involved with CL generation, U and Th zonation will control the density of radiation damage, and may therefore affect the quenching of the CL.

Low magnification inspection of FCT zircons using an optical microscope mounted CL system (CITL Technosyn 8200 Mk 4) indicate that they exhibit strong blue broad-band CL emission, and the majority of crystals show blue luminescent cores mantled by greener rims (Dobson, 2006). High-magnification panchromatic CL images of FCT zircons were obtained from a polished grain mount using a K.E. Developments Centaurus CL detector mounted on a Quanta FEI 200F Environmental Scanning Electron Microscope.

Primary magmatic concentric zonation patterns have previously been observed in BSE images of FCT zircons (Lamphere and Baadsgaard, 2001; Reiners et al., 2002). To avoid potential bias caused by the geometry of concentric zonation, and to ensure accurate determination of the position of zone boundaries, zonation characterisation was only performed on complete crystals sectioned parallel to the c-axis. Panchromatic images of over 400 c-axis parallel crystals were obtained under constant

instrumental operating and image capture conditions, and were used to assess the zonation styles within the crystal population.

A wide variety of CL zonation was observed, and crystals showing broadly similar zonation patterns still exhibit substantial inter-crystalline variation in CL intensity (Fig. 2, Table 1). The majority of crystals (86%) exhibited broadly concentric oscillatory zonation, but substantial variation in zone width, and relative intensity changes between adjacent zones was observed. These crystals can be subdivided by zonation style into two types. Type 1 zircons have a relatively large core of low CL intensity, typically 40-70% crystal width. This is mantled by a rim of moderate-to-high CL intensity that contains a number of zones with low CL intensity (Fig. 2a). The width, and rim relative position of the low CL intensity zones varies between crystals, but all crystals exhibit a relatively small, generally bimodal range of CL intensities. Type 2 zircons also have large cores and exhibit generally bimodal CL intensities. However, they generally have less extreme CL intensities than Type 1 zonation (Fig. 2b), and the low-to-moderate CL cores are surrounded by rims of moderate-to-high CL intensity that contain a few, narrow (<5 μm) zones of much lower CL intensity.

The remaining 12% of the c-axis parallel population show a variety of different zonation styles. Type 3 (6%) zircons have Type 1 or Type 2 zonation that is influenced by fluid or mineral inclusions (Fig. 2c). The large inclusions found in Type 3 crystals are visible at picking magnification (up to 500x). Inclusions can contain significant volumes on non-lattice generated He, and although this usually has minimal affect on zircon (U-Th)/He ages, Type 3 crystals would not be routinely selected for (U-Th)/He analysis. Type 4 and Type 5 crystals have simple zonation that can be approximated as a step function. Type 4 crystals have a moderate-low

intensity core mantled by a moderate-high intensity rim (Fig. 2d), while Type 5 exhibit a similar range of CL intensities, but the cores have higher CL intensity than the rims (Fig. 2e). Only 2% of the crystal population exhibited approximately homogenous CL intensity (Type 6; Fig. 2f).

The bi-alkali tube of the Centaurus CL detector is sensitive to wavelengths in the range 300-650nm, peaking in the blue spectrum. The wavelength limitations and peak sensitivity of the CL detector will affect the images produced, but the net CL signal used to generate panchromatic images is dominated by the broad-band emission (Kempe et al., 2000; Nasdala et al., 2003). Bias introduced by the non-linear response of the detector is therefore thought to be limited given the dominance of blue CL emission observed on the optical microscope CL system.

CL intensities for all zonation styles were quantified by translating the panchromatic images into greyscale colour space. The quantification of the panchromatic images can also be effected by a number of phenomena relating to the image capture conditions. High CL intensities may lead to saturation of the panchromatic image, whereas low CL emission may be below the detection threshold. Optimal image capture conditions were selected to maximise the range of greyscale values in the panchromatic image, and to minimise saturation. While good rendition of greyscale variations at both ends of the intensity scale was generally achieved under the optimal configuration, high CL zones in a few crystals showed very little greyscale variation, which suggests possible saturation. It is also possible that some variation at very low light intensities was overlooked. The optimisation of the image capture conditions does not change the inherent nonlinearity of the CL detector, and some bias towards enhanced emission intensity at wavelengths close to peak detection sensitivity is inevitable.

2.2. Correlation of CL intensity with U-Th distribution

The distribution of U and Th in the FCT zircons was measured using a Cameca ims 4f Ion Microprobe, with a 5-7μm pit diameter. Cycles of 10 measurements were made using an energy window of 40 eV and an energy offset of 75 V (Wiedenbeck et al., 2004). U and Th concentrations were calculated using the NIST SRM 610 standard glass with U = 461 ppm and Th = 458 ppm. U, Th and a range of trace elements (Y, Ce, Dy, Yb, Hf) were measured at 15 spots (Table 2) across three FCT zircons (Type 1, Type 2 and Type 5) and the full range of CL intensities. Crystal edges and crystals with narrow CL zonation patterns were avoided to minimise potential interference effects caused by analysis of multiple zones. In addition, U, Th, Y, Ce and Hf concentrations were measured along a c-axis parallel traverse across a fourth FCT zircon, selected for its typical broad Type 1 zonation (Table 3).

The concentration of U and Th in all crystals follows the zonation in CL, with U and Th concentrations increasing with decreasing CL intensity. The traverse records large changes in U and Th concentration between adjacent spots (Fig. 3, Table 3), which suggests that the spatial resolution of the ion beam (5-7 μm) is sufficient to prevent excessive interference from multiple zones at any site. The precise location and width of the zone boundary is beyond the 5-7 μm spatial resolution of the ion beam, but the CL images show that most zone boundaries are non-gradational concentration step functions.

The inter- and intra-crystalline correlation between CL intensity and U and Th concentration across the full range of CL emission intensities is shown in Fig. 4. The elemental concentration of U and Th can be related to the α-radiation damage density using the effective U concentration (eU), which incorporates the different alpha

productivity of U and Th (eU = [U] + 0.24 x [Th]). The relationship between CL intensity and eU concentration can be fitted by a regression curve of the form $y = a x^b$ ($R^2_{[eU]}$= 0.69), and although the physical basis for the application of this form of best-fit curve is not clear, it illustrates the strength of the correlation.

The distribution of Dy, Ce, Yb and Y in the FCT zircons generally follows U and Th (Fig. 3, Tables 2 and 3), but correlations between CL intensity and the trace element concentrations are generally less well defined than with eU. This is consistent with panchromatic images dominated by broad-band CL emission (Kempe et al., 2000). Dy is a major controls of narrow-band CL generation in zircon (Corfu et al., 2003; Ewing et al., 2003; Nasdala et al., 2003), and the interplay between narrow-band CL generation at Dy centres and a radiation controlled quenching processes can be illustrated in the form of Dy/eU. A positive correlation between net CL intensity and Dy/eU exists in the FCT zircons (Fig. 5), but further spectral analysis and compositional data is required before this relationship can be correctly interpreted.

Studies using doped and synthetic crystals to investigate CL in zircon suggest that multiple mechanisms control the generation and quenching of the CL signal (Ewing et al., 2003; Nasdala et al., 2003). However, the correlation shown here may indicate that in natural, relatively young samples the amount of radiation damage, as indicated by the eU concentration, may be a dominant factor in controlling the net emission intensity. Analyses of a broader set of samples is required before this can be corroborated.

Scatter on the correlation between eU and CL intensity may be caused by the spatial resolution of the ion beam. In some instances, two or more zones may have been sampled in a single analysis; as illustrated by the two spot analyses (Table 2) performed on sites where the beam is known to interact with an area of moderate CL

intensity, cut by a narrow (<2 μm) zone of low CL intensity. These sites have eU concentrations higher than predicted from the average CL intensity of the site. However, they are consistent with the large contribution to the total signal that comes from the relatively small volume low CL (high eU) zone. Scatter may also be caused by the different crystal volume involved with the generation of the CL signal and that sampled by the ion-beam. Despite this, the correlation between eU and net CL intensity means that, at least for zircons from the FCT, CL zonation can be used as a first order, semi-quantitative approximation of U and Th zonation within a population.

Detailed quantitative mapping and accurate characterisation of U and Th zonation in individual zircons is not routinely performed prior to (U-Th)/He analysis (Farley, 2002; Reiners 2005). This is because complete, undamaged crystals are used for (U-Th)/He analysis. The preparation of polished sections required for most quantitative techniques, and damage caused by analysis prevents individual crystals from being dated by (U-Th)/He after U and Th zonation has been quantitatively assessed. It is possible to assess U zonation in a sample using variation in fission track densities. However, this technique is insensitive on the small length scales (<10μm) required to resolve zone boundaries, and to small absolute concentration changes across zone boundaries. Assessing U and Th distributions in a crystal population using the CL proxy therefore offers improved understanding of zonation within a crystal population, and provides a population based method for assessing the effect of U-Th zonation on any individual (U-Th)/He analysis.

3. DISCUSSION

For zircons with a homogeneous U and Th distribution the proportion of He lost by α-ejection is calculated using an empirical relationship between fractional retention (F_T) and the surface area-to-volume ratio (β) of the crystal:

$$F_T = 1\text{-}a\,\beta + b\,\beta^2 \quad (1)$$

where a and b are constants that incorporate the density of the mineral and the energy of the decay (Farley et al., 1996; Hourigan et al., 2005). For tetragonal zircon crystals with two pyramidal terminations a = - 4.281 b = 4.372 for ^{238}U, and a = - 4.869 and b = 5.605 for ^{235}U and ^{232}Th (Hourigan et al., 2005).

Variable U and Th zonation in FCT zircons will cause dispersion in the measured (U-Th)/He ages, as each crystal will have lost a different fraction of He through α-ejection. This age dispersion will be maintained, or even compounded, by assuming homogeneity when calculating the α-ejection correction. The geometry and zonation specific ejection corrections (F_Z) for each of the zonation types can be calculated using the model developed by Hourigan et al., (2005). The error introduced by applying a homogenous F_T correction can be quantified using the concept of age bias, which has been defined by Hourigan et al (2005) as:

$$\gamma = F_T/F_Z - 1 \quad (2)$$

where F_T and F_Z are calculated for the same crystal geometry.

Twenty five CL intensity profiles (Fig. 1a. Electronic Appendix 1) were measured across typical examples of each of the zonation styles (except Type 3). Although limited to 25 profiles by computational constraints, effort was made to ensure that the chosen profiles represented the wider population, and 20 profiles of Type 1 and Type 2 crystals were selected at random from the entire Type 1 and Type 2 population. This included two profiles of Type 2 crystals where the low CL zones in the crystal

rim were too narrow and numerous to measure accurately. In this case the average CL intensity across the rim was used (Profiles 13 & 14, Fig. EA1a). To assess the age bias introduced by Type 4 and Type 5 crystals, profiles were measured on the crystals with the minimum and maximum CL intensity change, and the widest and narrowest rim thickness. It should be noted that more extreme zonation may exist in a larger crystal population. Type 6 crystals were not modelled as they have a zero age bias.

The width of each zone was measured from core-to-rim along the c-axis of the crystal. All zonation types are seen in all crystal size fractions, and zone widths generally scale with crystal size. FCT crystals selected for (U-Th)/He analysis generally have diameters between 50 and 150μm, and so to identify possible variation in age bias with crystal size, the rim relative positions for each zone boundary were used to scale each zonation profile to three different crystal sizes (XL_1: width = 50μm, total length = 160μm, termination height = 30μm, XL_2: width = 100μm, total length = 200μm, termination height = 30μm, and XL_3: width = 150μm, total length = 250μm, termination height = 50μm).

The scatter in the relationship between CL intensity and eU, U and Th (Fig. 4) complicates the estimation of the U and Th concentration profile. However, as the majority of the crystals show only a limited number of distinct CL intensities, and each zone shows a range of greyscale vales (typically 10-15 greyscale units) a number of CL intensity bins were defined. Each of these intensity bins was assigned an average U and Th concentration using the relationships shown in Fig. 4, and the simplified concentration profiles constructed. This simplification allows the zonation profiles for any crystal to be easily estimated, but means that U and Th concentrations for any individual zone or CL intensity may be over- or under-estimated, but these

effects should largely cancel out. The validity of this simplification can be illustrated by the small differences in the eU (Fig. 6a) and age biases (Fig. 6b) between the two core-rim profiles constructed from the SIMS traverse (Fig EA1b) and the profiles estimated from the greyscale values. The difference between the age bias of the measured and estimated profiles is less than ± 2.5%, with the largest difference occurring for large crystals. At smaller crystal sizes more zones fall in the region affected by ejection meaning there is a greater averaging effect.

For most of the model zonation profiles the age bias falls between +10% (i.e. F_T-corrected ages are 10% too old) and -5% (i.e. F_T-corrected ages are 5% too young) (Fig. 7a). The profiles generated from the ion probe traverse data have age biases that fall within the range of the profile models (Fig. 6). This crystal was selected for detailed analysis because of its broad zones and wide spectrum of CL intensities, and this is reflected in the somewhat extreme age bias at small crystal sizes. The models with Types 4 and 5 zonation have age biases of up to ± 25 % (Fig. 7a), which may explain the occasional extreme age in the dataset (Fig. 1).

The modelling highlights the dependence of age bias on crystal size (Fig. 7b). Larger crystals generally have more negative, and less extreme age bias than smaller crystals. The width of the zone affected by α-ejection does not change, while the width of the individual zones scales with the crystal dimensions. Therefore the size-related skew on the age bias data is a reflection of the relative volume affected by α-ejection in large crystals, and the increased averaging effect in small crystals where several zones are affected by ejection.

The model profiles were a representative sample of Type 1 and Type 2 zonation, so the range in age bias from the model profiles is assumed to be reflective of the entire population of Type 1 and Type 2 crystals. When coupled to the age biases determined

on Type 4 and Type 5 zonation, it is therefore possible to extrapolate the population statistics and assess the effect of F_T-correction on a large (U-Th)/He dataset (Fig. 7c). Consideration of an extended zonation-type weighted dataset (Fig. 7c & d, using 100 crystals of each size fraction) suggests that the F_T-corrected (U-Th)/He ages will have a mean age bias of +3.6 ± 11.0% (2σ). This implies that the α-ejection corrected dataset slightly over-estimates the true zircon (U-Th)/He age of the FCT by ~ 1 Myr, and the correct age should be 27.5 ± 3.1 Ma. This is still within error of the reported fission track, Ar/Ar and U/Pb ages (Hurford and Hammerschmidt, 1985; Carpéna and Mailhé, 1987; Schmitz and Bowring, 2001; Renne et al., 2004). Crucially, this work explains why the F_T-corrected ages only have a reproducibility of approximately ± 11 %.

This study questions the applicability of FCT zircon as a mineral age standard for (U-Th)/He studies. FCT zircons exhibit strong and variable oscillatory CL zonation that corresponds to equally strong and variable U and Th zonation. The age reproducibility of the FCT zircons is therefore not representative of that which would be expected from crystals with sector zonation, narrow, or subtle oscillatory zonation. The age reproducibility of zircons with more homogenous U and Th distributions, or where the ejection correction is less important is largely untested. However, these samples would better test the limits of the methodology, and perhaps provide a less variable age standard for inter-laboratory correlation. Preliminary zonation studies of zircons from the Tardree Rhyolite (Hourigan et al., 2005; Tagami et al., 2003) and Muck Tuff (Dobson, 2006) show that a consistent α-ejection is applicable, or at least that F_Z-correction can be confidently estimated (Dobson, 2006).

This study highlights the importance of characterising the U and Th distribution in before applying the α-ejection correction or interpreting zircon (U-Th)/He ages. The

use of CL images to assess the zonation within a population appears to allow a qualitative assessment of the U and Th zonation in zircon. For some samples this may significantly reduce the scatter in the (U-Th)/He age distribution, and, where CL zonation is dependant on crystal geometry or size, may allow additional crystal selection criteria to be used to optimise the reproducibility of the (U-Th)/He ages.

4. CONCLUSIONS

Characterisation of the U and Th distribution in zircon crystals used for (U-Th)/He dating is not routinely performed. However, without qualitative and quantitative investigation, the scatter observed in F_T-corrected (U-Th)/He ages will remain, the age bias introduced by inaccurate ejection-correction cannot be assessed, net age biases may be overlooked, and data will continue to be discarded because of apparently poor sample reproducibility. We advocate the use of the CL zonation population statistics to estimate the potential distribution of measured (U-Th)/He ages within a zircon population, in an effort to improve our understanding of zircon (U-Th)/He datasets. We also suggest that the practice of presenting all (U-Th)/He ages in their F_T-corrected form should be reappraised. Modelling techniques and data interpretation of apatite and zircon (U-Th)/He ages no longer require F_T-corrected values (Dunai, 2005; Hourigan et al., 2005; Ketcham, 2005; Meesters and Dunai, 2002), and we suggest that reporting the uncorrected age, and the dimensions or surface area-volume ratio of the crystal would allow greater transparency, and remove the potential error introduced by inaccurate ejection correction.

Acknowledgements: This study was supported by NERC Ph.D. award NER/S/A/2002/10370 and STATOIL. Ray Donelick supplied the FCT zircons. We thank Richard Hinton for assistance at EMIF, and Jurgen Foeken, Valerie Olive and David Vilbert for assistance in the laboratory. Bernard Marty and two anonymous reviewers are thanked for their constructive comments that have helped improve this manuscript. The SUERC He laboratory is supported by the Scottish Universities.

REFERENCES

Carpéna J. and D. Mailhé (1987) Fission-track dating calibration of the Fish Canyon Tuff standard in French reactors. *Chem. Geol.* **66**, 53-59.

Corfu F., Hanchar J. M., Hoskin P. W. O., and Kinny P. (2003) Atlas of zircon textures. *Rev. Mineral. Geochem.*, **53**, 468-500.

Dobson K. J. (2006) The zircon (U-Th)/He thermochronometer: development and application of thermochronometers in igneous provinces, University of Glasgow. Ph.D. Thesis, University of Glasgow.

Dunai T. J. (2005) Forward modeling and interpretation of (U-Th)/He ages. *Rev. Mineral. Geochem*. **58,** 259-274.

Edwards P. R., Martin R. M., and Lee M. R. (2007) Combined cathodoluminescence hyperspectral imaging and wavelength dispersive X-ray analysis of minerals. *Am. Mineral.* **92**, 235-242.

Ewing R. C., Meldrum A., Wang L. L., Webber W. J., and Corrales L. R. (2003) Radiation effects in zircon. *Rev. Mineral. Geochem.* **53,** 387-425.

Farley K. A. (2002) (U-Th)/He dating: techniques, calibrations, and applications. *Rev. Mineral. Geochem*. **47,** 819-843.

Farley K. A., Wolf R. A., and Silver L. T. (1996) The effects of long alpha-stopping distances on (U-Th)/He ages. *Geochim. Cosmochim. Acta* **60**, 4223-4229.

Hanchar J. M. and Miller C. F. (1993) Zircon zonation patterns as revealed by cathodoluminescence and backscattered electron images: Implications for interpretation of complex crustal histories. *Chem. Geol.* **101**, 1-13.

Hourigan J. K., Reiners P. W., and Brandon M. T. (2005) U-Th zonation-dependent alpha-ejection in (U-Th)/He chronometry. *Geochim. Cosmochim. Acta* **69**, 3349-3365.

Hurford A. J. and Hammerschmidt K. (1985) 40Ar/39Ar and K/Ar dating of the Bishop and Fish Canyon Tuffs: Calibration ages for fission-track dating standards. *Chem. Geol.* **58**, 23-32.

Kempe U., Gruner T., Nasdala L., and Wolf D. (2000) Relevance of cathodoluminescence for the interpretation of U-Pb zircon ages, with an example of an application to a study of zircons from the Saxonian Granulite Complex, Germay. In. *Cathodoluminescence in Geosciences* (eds. Pagel M., Barbin V., Blanc P., and Ohnenstetter D.,) Springer-Verlag, Berlin-Heidelberg, pp 415-455

Ketcham R. A. (2005) Forward and inverse modeling of low-temperature thermochronometry data. *Rev. Mineral. Geochem.*. **58**, 275-314.

Lamphere M. A. and Baadsgaard H. (2001) Precise K–Ar, $^{40}Ar/^{39}Ar$, Rb–Sr and U/Pb mineral ages from the 27.5 Ma Fish Canyon Tuff reference standard. *Chem. Geol.* **175**, 653-671.

Meesters A. G. C. A. and Dunai T. J. (2002) Solving the production-diffusion equation for finite diffusion domains of various shapes - Part II. Application to cases with alpha-ejection and nonhomogeneous distribution of the source. *Chem. Geol.* **186**, 57-73.

Nasdala L., Zhang M., Kempe U., Panczer G., Gaft M., Andrut M., and Polotze M. (2003) Spectroscopic methods applied to zircon. *Rev. Mineral. Geochem*. **53,** 427-467.

Reiners P. W. (2005) Zircon (U-Th)/He thermochronometry. *Rev. Mineral. Geochem*. **58**, 151-179.

Reiners P. W., Farley K. A., and Hickes H. J. (2002) He diffusion and (U-Th)/He thermochronometry of zircon: initial results from Fish Canyon Tuff and Gold Butte. *Tectonophys.* **349**, 297-308.

Reiners P. W., Spell T. L., Nicolescu S., and Zanetti K. A. (2004) Zircon (U-Th)/He thermochronometry: He diffusion and comparisons with $^{40}Ar/^{39}Ar$ dating. *Geochim. Cosmochim. Acta* **68**, 1857-1887.

Renne P. R., Deino A. L., Walter R. C., Turrin B. D., Swisher C. C., Becker T. A., Curtis G. H., Sharp W. D., and Jaouni A. R. (1994) Intercalibration of astronomical and radioisotopic time. *Geology* **22**, 783-786.

Remond G., Cesbron F., Chapoulie R. Ohnenstetter D., Roques-Carmes C., and Schvoerer M., (1992) Cathodoluminescence applied to the microcharacterization of mineral materials: a present status in experimentation and interpretation. *Scanning. Microsc. Intl.* **6**, 23-68

Schmitz M. D. and Bowring S. A. (2001) U-Pb zircon and titanite systematics of the Fish Canyon Tuff: an assessment of high-precision U-Pb geochronology and its application to young volcanic rocks. *Geochim. Cosmochim. Acta* **65**, 2571-2587.

Tagami T., Farley K. A., and Stockli D. F. (2003) (U-Th)/He geochronology of single zircon grains of known Tertiary eruption age. *Earth Planet. Sci. Lett.* **207**, 57-67.

Wiedenbeck M., Hanchar J. M., Peck W. H., Sylvester P., Valley J., Whitehouse M., Kronz A., Morishita Y., Nasdala L., Fiebig J., Franchi I., Girard J. P.,

Greenwood R. C., Hinton R., Kita N., Mason P. R. D., Norman M., Ogasawara M., Piccoli P. M., Rhede D., Satoh H., Schulz-Dobrick B., Skar O., Spicuzza M. J., Terada K., Tindle A., Togashi S., Vennemann T., Xie Q., and Zheng Y. F. (2004) Further Characterisation of the 91500 Zircon Crystal. *Geostandards & Geoanalytical Res.* **28**, 9-39.

Table 1. Description of cathodoluminescence zonation patterns observed within the c-axis parallel crystals of the FCT zircon population.

Zonation Type	Proportion	Core	Rim	Notes
Type 1 Complex High Contrast	**48 %**	Large, homogeneous low CL intensity. Often single broad band of slightly higher CL intensity within core region.	Moderate-high CL intensity. Several 1-15μm zones of low CL intensity. Variable rim-relative position	Large range of CL intensities, variable zone widths in population but narrow (generally bi-modal) range of CL intensities in each individual crystal. Rim relative position of the low CL zones is highly variable. Low CL zones are generally broader than for Type 2 crystals.
Type 2 Complex Moderate Contrast	**38 %**	Single moderate to high CL intensity with several narrow (<5 μm), low CL intensity zones. Low CL intensity cores in some crystals	Less variation in zone widths, and smaller relative intensity changes across zone boundaries than in Type 1. Rim relative position of the low CL zones is highly variable. Generally bi-modal range of CL intensities	
Type 3 Inclusion Influenced	**6 %**	As for Type 1 and Type 2 with zonation influenced by inclusions. Inclusions generally in crystal cores. Would not be selected for (U-Th)/He analysis		
Type 4 Lower Core Step	**2 %**	Homogeneous moderate CL intensity	Homogeneous moderate-high CL intensity, typically 20-25 μm wide	A simple step-function zonation. Limited range of CL intensity.
Type 5 Lower Rim Step	**2 %**	Homogeneous moderate-high CL intensity	Homogeneous moderate CL intensity, typically 20-25 μm wide	Same general structure as Type 4, but the CL intensities are reversed. Limited range of CL intensity.
Type 6 Approximately Homogenous	**2 %**	Moderate-low CL intensity, very subtle narrow oscillatory zonation.	Indistinct core-rim boundary, orientation of the zonation in the cores suggests a xenocrystic origin for these crystals	

Table 2**.** Ion probe U, Th and trace element analyses from FCT zircon.

	FCT1-1	FCT1-2	FCT1-3	FCT1-4	FCT1-5	FCT1-6	FCT2-1	FCT2-2	FCT2-3	FCT2-4	FCT2-5	FCT2-6	FCT2-7	FCT2-8	FCT3-1
CL Int.[*]	55	30	45	60	50	50	220	160	77	185	170	242	235	125	250
U (ppm)	169	5098	440	191	1371	3637	84	62	232	210	101	73	50	121	15
error	*0.9%*	*0.2%*	*0.5%*	*0.8%*	*0.3%*	*0.0%*	*1.4%*	*1.6%*	*0.9%*	*0.8%*	*1.1%*	*1.3%*	*1.6%*	*1.0%*	*3.8%*
Th (ppm)	444	4381	523	612	1132	3195	137	210	600	248	140	126	95	162	51
error	*0.6%*	*0.2%*	*0.5%*	*0.5%*	*0.4%*	*0.1%*	*1.2%*	*0.9%*	*0.6%*	*0.8%*	*1.0%*	*1.1%*	*1.3%*	*1.0%*	*2.3%*
eU[¶]	613	9479	963	802	2503	6832	222	272	833	458	241	199	144	283	67
Trace elements[#]															
Y (ppm)	542	6672	2427	1232	1116	9248	1243	691	592	2955	1434	1256	1048	1820	369
Ce (ppm)	44	715	147	71	145	735	49	39	61	120	55	46	39	65	23
Dy (ppm)	36	698	261	136	135	1022	134	48	41	364	166	133	108	239	29
Yb (ppm)	259	2190	752	509	529	2865	419	297	350	808	457	397	322	561	126
Hf (ppm)	11801	9490	10697	9032	12148	9210	7675	9264	14200	8243	7955	7609	8132	8475	10090

[*]Spot averaged monochromatic greyscale CL intensity

[¶]Effective uranium eU=[U]+0.24*[Th]

[#]Analytical error on trace element data of ± 2.0%

Table 3. Ion probe U, Th and trace element analyses from a traverse of a FCT zircon (Fig. 3).

Distance (μm)	CL Intensity*	U# (ppm)	Th# (ppm)	eU¶ (ppm)	Y#(ppm)	Ce# (ppm)	Hf# (ppm)
Traverse Data							
0	199	559	295	630	606	54	10217
5	98	718	383	810	929	73	9375
10	74	572	261	634	650	58	10205
15	78	434	181	478	523	45	10565
20	132	712	416	812	471	48	10753
25	29	3071	3567	3927	2032	240	9858
30	22	3221	3620	4089	4405	426	7886
35	32	2484	1813	2919	3853	245	7593
40	16	3304	3288	4093	4302	389	8388
45	40	1920	1676	2323	2760	267	10020
50	118	562	296	633	827	72	10844
55	78	583	239	641	652	56	10180
60	73	778	367	866	1156	82	9381
65	88	863	424	965	1516	106	9334
70	78	798	418	898	1481	102	9240
75	118	535	286	604	827	57	9773
80	98	427	183	471	469	45	10112
85	108	410	168	451	395	31	9996
90	88	1072	903	1288	741	64	9375
95	88	579	336	660	592	46	9412
100	147	558	312	633	415	28	9952
105	78	498	282	566	453	35	9789
110	196	288	127	318	399	26	7135
Additional spot analyses							
1§	87	569	211	780	817	47	11564
2§	104	857	501	1358	940	75	11938

*Spot averaged monochromatic greyscale CL intensity determined using standard graphics software.

#Analytical error on all element data ± 2.0%

¶ Effective uranium eU = [U]+0.24*[Th]

§ Spot analyses placed to intersect more than one zone (see Fig.3)

FIGURE CAPTIONS

Fig. 1. a) (U-Th)/He ages of the Fish Canyon Tuff zircon (n = 129) from laboratories routinely making measurements. Open diamonds – Yale (Reiners, 2005), open squares – California Institute of Technology (Tagami et al., 2003), open triangles – CPRG, Nancy (in Dobson, 2006), filled diamonds – S.U.E.R.C. (Dobson, 2006). All error bars are 2σ. The two zircon (U-Th)/He ages younger than 20 Ma are not included in the average age calculation as these samples are through to be affected by an extreme form of U and Th zonation (Tagami et al., 2003; Dobson 2006). The average age of the FCT zircons is 28.3 ± 3.1 Ma (± 10.9%, 2σ, n = 127). b) Histogram showing the distribution of FCT zircon (U-Th)/He ages.

Fig. 2. The six different types of cathodoluminescence zonation observed in the FCT zircons. For detailed descriptions of different zonation styles, see text and Table 1. a) Type 1, b) Type 2, c) Type 3, d) Type 4, e) Type 5, f) Type 6. All scale bars are 50 μm. Images captured under the identical operating conditions (high vacuum, constant spot size and operating voltage (30kV), brightness and contrast settings). Types 1-4 show complete crystals, but incomplete crystals of Type 5 and Type 6 are shown as these were the best quality images obtained. The bright linear features visible in the images of Types 2 and 6, and also Type 1, are associated with charging of the sample along cracks or scratches in the polished surface (Schmitz and Bowring, 2001).

Fig. 3. a) CL image of crystal used for SIMS traverse taken after ion probe analyses showing the location of the traverse and the additional spot analyses (Table 3). b) Detailed schematic map of the CL intensity variation along the traverse. c) U, Th and trace element concentrations determined on the ion probe.

Fig. 4. The correlation between CL intensity and U (filled diamonds), Th (hollow diamonds) and effective Uranium (eU; filled squares) concentration for all ion probe analyses. Regression curves have the form ax^b and have $R^2_{[U]} = 0.63$ (a = 398,800, b = -1.51, $R^2_{[Th]} = 0.78$ (a = 241,700 b = -1.43), $R^2_{[eU]} = 0.69$ (a = 428,850, b = -1.48).

Fig 5. The relationship between Dy/U, Dy/Th and Dy/eU with CL intensity for each of the spot analyses performed on the Fish Canyon Tuff zircons.

Fig. 6 a). The correlation between relative eU measured on the SIMS traverse and estimated from the greyscale values. b) The age bias calculated for the 2 U-Th profiles measured on the SIMS (diamonds) and the model profiles estimated from the greyscale values (squares) for each of the three crystal sizes (see text for details). XL_1 - black symbols, XL_2 - grey symbols, XL_3 - white symbols. Measured zonation profiles can be found in Fig. EA1b.

Fig. 7. Predicted age bias in the FCT zircon population. Zonation models can be found in Fig. EA1a. In all panels XL_1 - black diamonds, XL_2 grey diamonds, XL_3 white diamonds. Crystal dimensions are defined in the text. a) The predicted age bias for 25 model profiles. The model profiles can be found in Fig. EA1a. b) The predicted age bias for 25 model profiles for each of the three crystal sizes (see text for details). c) The predicted age bias for a randomly selected FCT crystal population with equal sampling (100 crystals) of each size fractions. d) Frequency distribution of the predicted age bias shown in Fig. 7c.

FIGURES

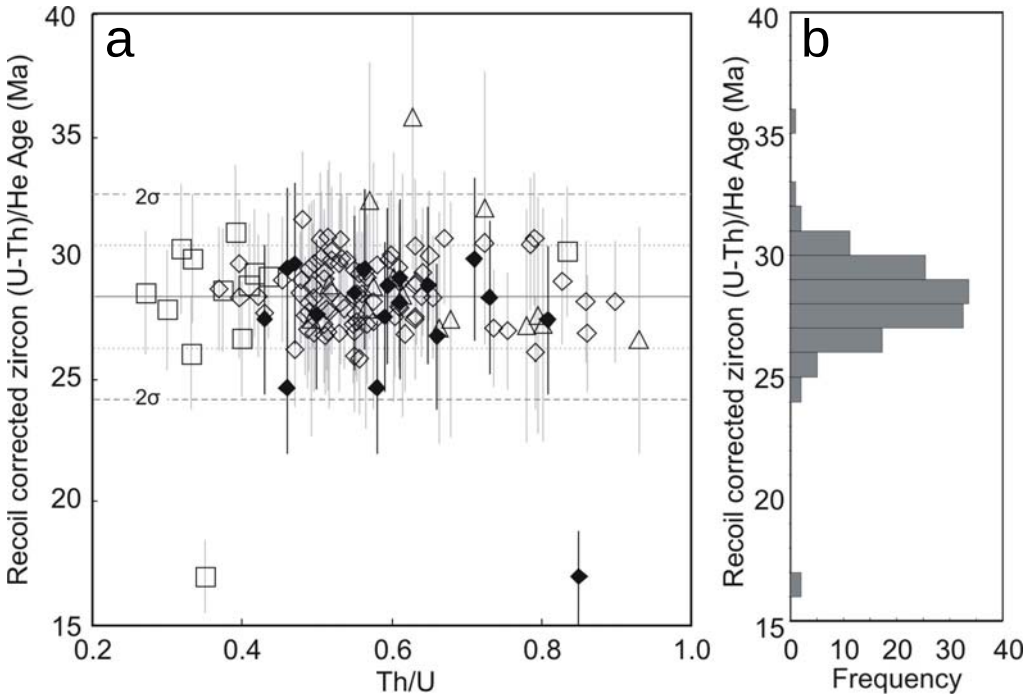

Fig.1.

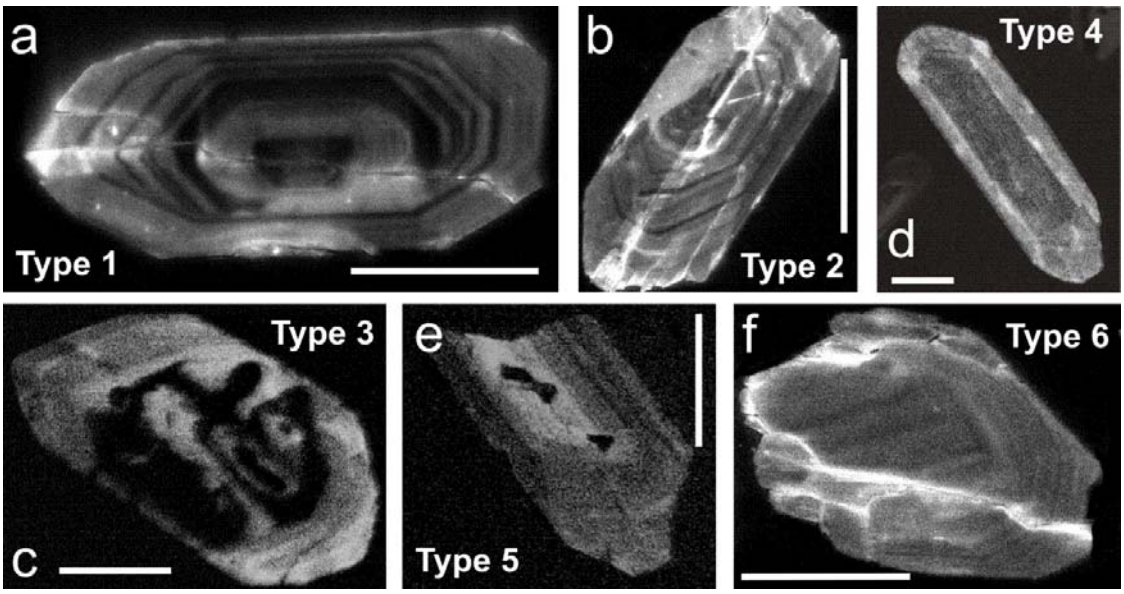

Fig. 2

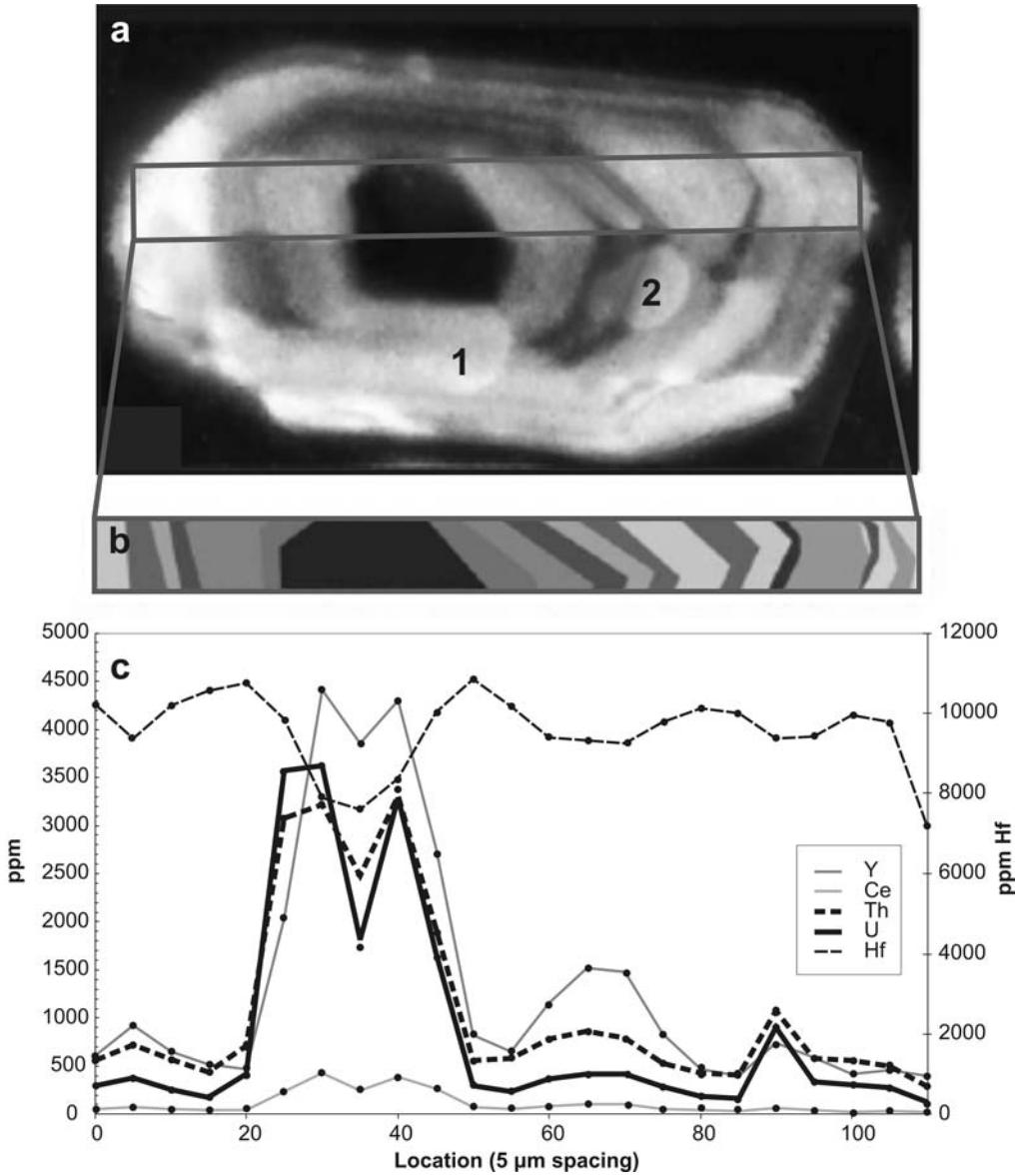
a
2
1
b
c
5000
4500
4000
3500
3000
2500
2000
1500
1000
500
0
ppm
12000
10000
8000
6000
4000
2000
0
ppm Hf
0
20
40
60
80
100
Location (5 µm spacing)
Y
Ce
Th
U
Hf

Fig. 3.

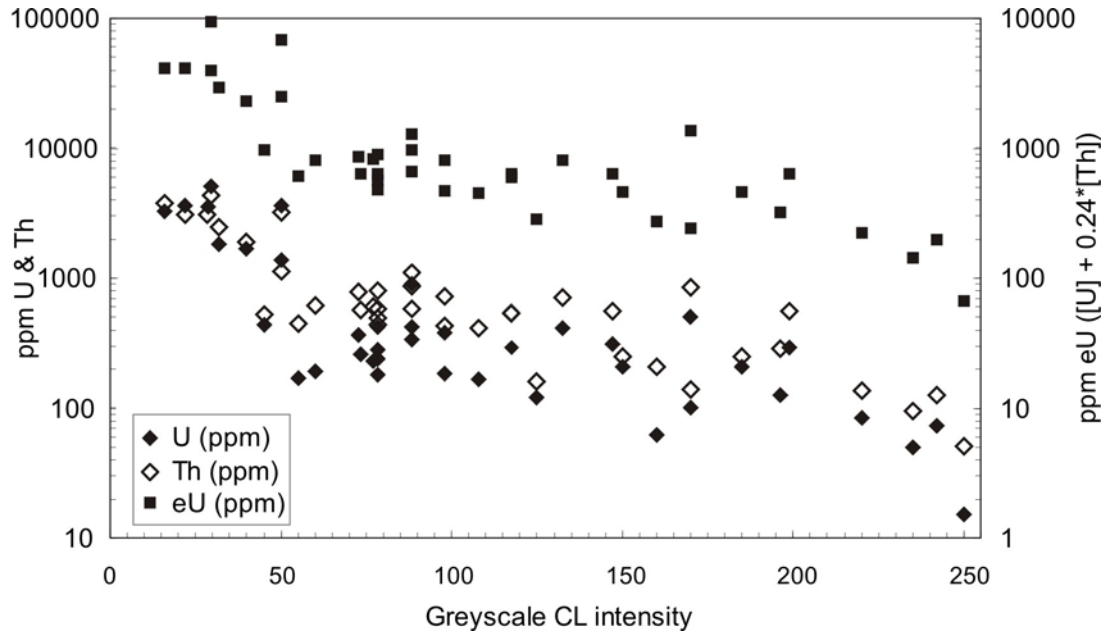
100000
10000
1000
100
10
ppm U & Th
10000
1000
100
10
1
ppm eU ([U] + 0.24*[Th])
U (ppm)
Th (ppm)
eU (ppm)
0
50
100
150
200
250
Greyscale CL intensity

Fig. 4.

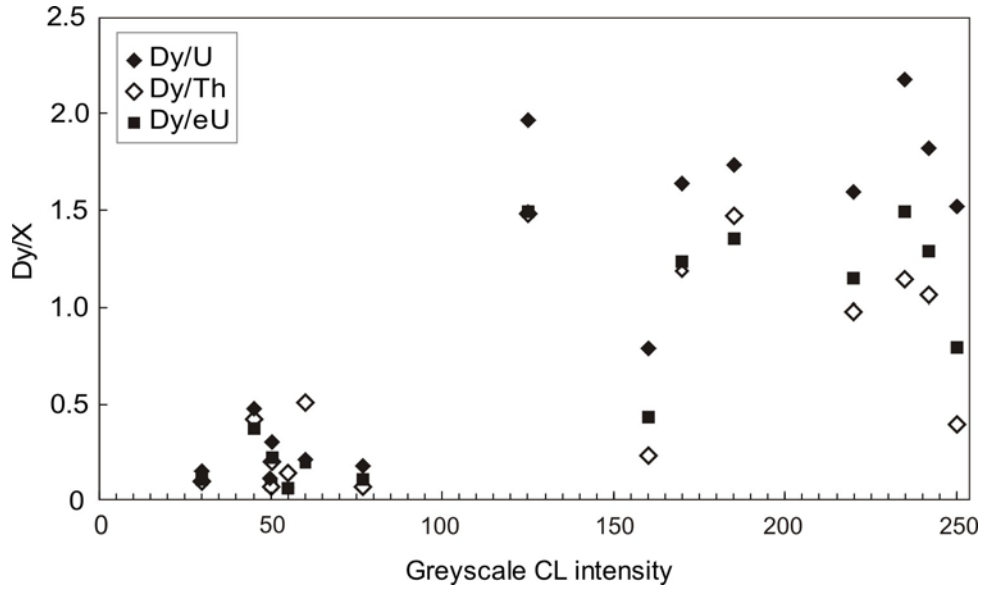
Dy/U
Dy/Th
Dy/eU
Dy/X
Greyscale CL intensity
0
0.5
1.0
1.5
2.0
2.5
0
50
100
150
200
250

Fig. 5.

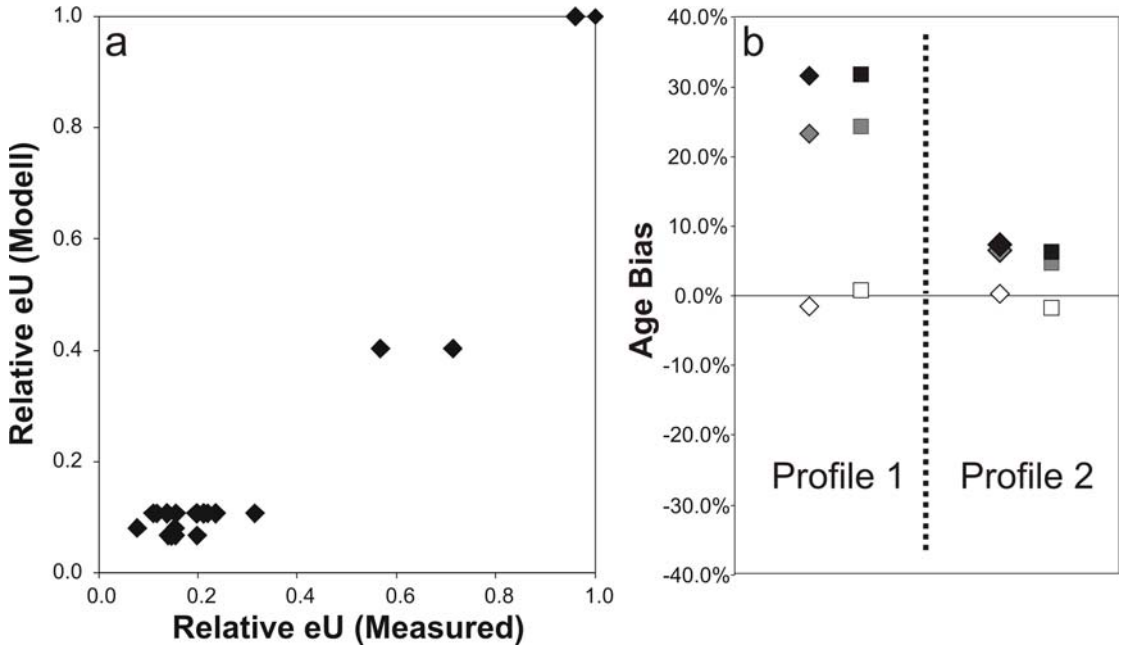
a
Relative eU (Modell)
Relative eU (Measured)
0.0
0.2
0.4
0.6
0.8
1.0
b
Age Bias
40.0%
30.0%
20.0%
10.0%
0.0%
-10.0%
-20.0%
-30.0%
-40.0%
Profile 1
Profile 2

Fig. 6.

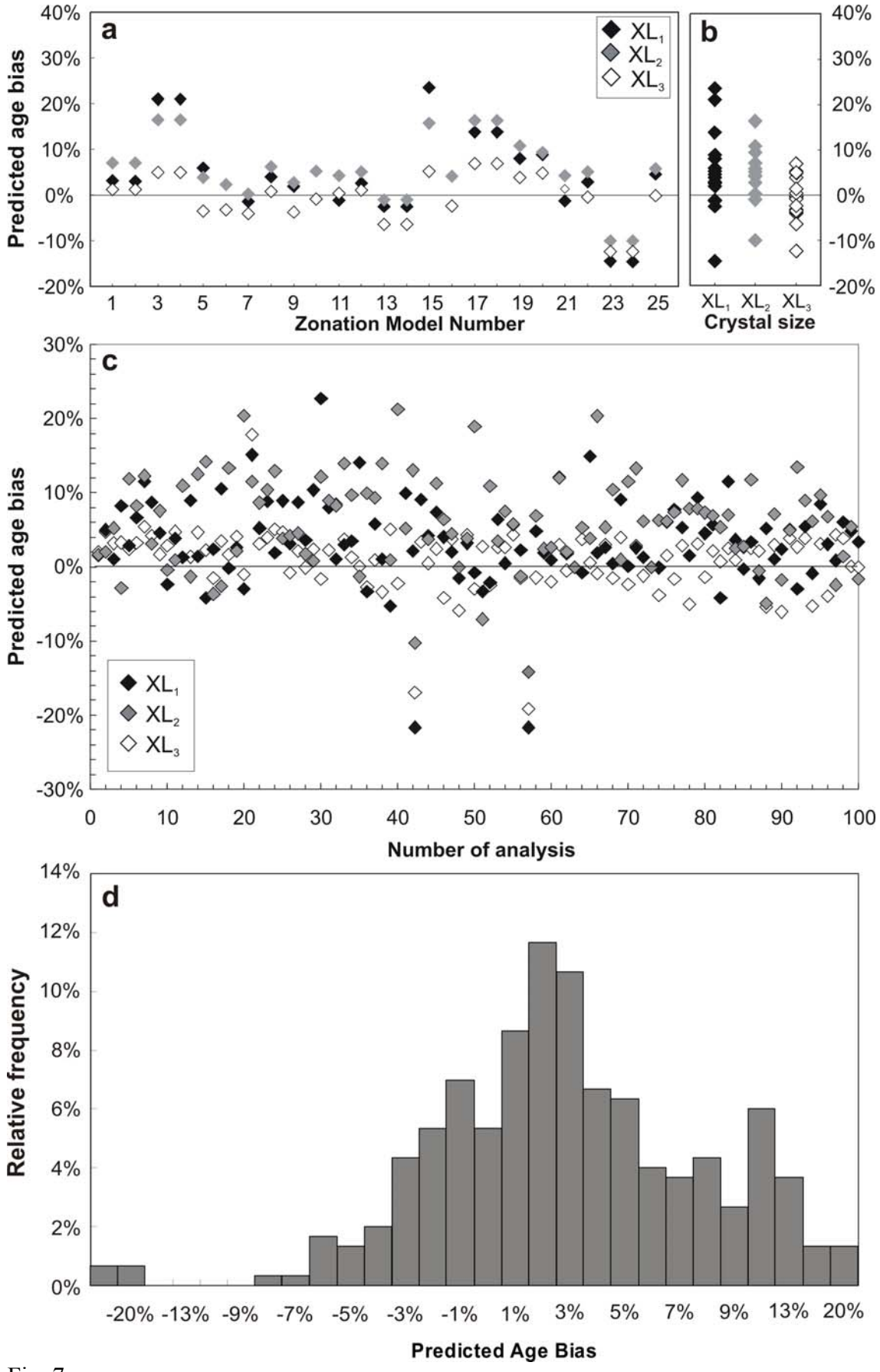
a
b
c
d
XL1
XL2
XL3
Predicted age bias
Zonation Model Number
Crystal size
Number of analysis
Relative frequency
Predicted Age Bias
40%
30%
20%
10%
0%
-10%
-20%
-30%
1
3
5
7
9
11
13
15
17
19
21
23
25
0
10
20
30
40
50
60
70
80
90
100
14%
12%
10%
8%
6%
4%
2%
0%
-20%
-13%
-9%
-7%
-5%
-3%
-1%
1%
3%
5%
7%
9%
13%
20%

Fig. 7.